The 3D Surface Crack-front Constraints in Welded Joints

Hyungyil Lee[1)]

1) Department of Mechanical Engineering, Sogang University, Seoul 121-742, Korea

ABSTRACT

Single parameter such as stress intensity factor K or J-integral in traditional fracture mechanics depends strongly on the geometry and loading condition. Therefore the second parameter like T-stress measuring the stress constraint is additionally needed to characterize the general crack-tip fields. While many research works have been done to verify the J-T description of elastic-plastic crack-tip stress fields in plane strain specimens, limited works (especially for bimaterials) have been performed to describe the structural surface crack-front stress fields with the two parameters. On this basis, via detailed three dimensional finite element (FE) analyses for surface-cracked plates and straight pipes of homogeneous materials and bimaterials, we investigate the extended validity or limitation of the two parameter approach. We here first develop a full 3-D mesh generating program for semi-elliptical surface cracks, and calculate elastic T-stress from the obtained FE stress field. We then confirm the extended validity of J-T methodology in characterizing the surface crack-front fields of welded plates and pipes under various loadings by comparing the J-T predictions to the elastic-plastic 3-D FE stress fields.

INTRODUCTION

The main role of the fracture mechanics is to describe the correlation between standard specimen fracture and macroscopic fracture of the cracked structure, throughout various crack-tip governing parameters. The toughness correlation between specimen and various cracked structures are based on "similarities" of crack-tip stress and strain fields. Traditionally, these crack-tip fields are described by such parameters as stress intensity factor K of elastic fracture mechanics, or J-integral of elastic-plastic fracture mechanics. Provided these K or J are certainly dominant at both specimen and structure crack-tip fields with the same material properties, the fracture of the structure can be predicted. However, the validity of these single parameters are limited by geometric configuration or loading conditions of the specimen. For these reasons, in addition to the single parameter, another parameter which reflects the geometric configuration and loading conditions is required in quantifying the crack-tip stress and strain fields.

Larsson and Carlsson [1] showed that the size and configuration of plastic zone at the elastic-plastic crack-tip are notably influenced by the second term of the Williams [2] eigen expansion of isotropic elastic crack-tip stress field. Inspired by this observation, Rice [3] analyzed the effects of the second term on the plastic zone using the two symmetrical shear-band model emanating from the crack-tip. Rice denoted the second term of eigen expansion the T-stress. By observing the crack-tip stress fields of strain hardening plane-strain specimen with diverse T-stresses, Betegon and Hancock [4] demonstrated that elastic-plastic crack-tip stress fields under small scale yielding (SSY) can be quantitatively described by the first two terms of Williams eigen expansion. In other words, the asymptotic crack-tip solution described above by the single parameter corresponds to the special case ($T > 0$) of more general solution described by two parameters J-T.

With this background, this work studies the effect of strength mismatch on the stress field of semi-elliptical surface cracks in the bimaterial plates and pipes, in terms of J-T. By comparing J-T predictions to the 3-D FE elastic-plastic stress fields, we investigate the extended validity of J-T parameter approach.

THREE DIMENSIONAL CRACK ANALYSIS PROGRAM

Flaws in engineering practice are encountered most frequently in the form of surface cracks. Due to their intrinsic three-dimensional nature, surface crack analysis problems are generally approached by numerical technique. However geometric and parametric complexities of surface crack make the routine application of 3-D FE analysis quite inconvenient. Particularly singular finite elements laid along the surface crack-front make the manual preparation of FE mesh almost prohibitive. To overcome these kinds of problems, we develop an automatic 3-D FE mesh generation program for plates and pipes with semi-elliptical surface cracks. We also prepare a post-processing program to efficiently calculate the value of second parameter T-stress along the crack-front, thereby predicting the stress by J-T two parameters.

Automatic 3D Finite Element Mesh Generation Program

We model only one quarter of the configuration, considering the geometric and load symmetries of plate and pipe with a semi-elliptical surface crack. The semi-elliptical surface crack is located on the center of the plate, and in the case of pipe, on the exterior of the pipe center (Fig. 1). The total length of the plate is $2h$, the width $2b$, and the thickness t. The total length of the pipe is $2h$, and the inner radius R, and the thickness t. Also, the maximum crack depth is a, and the crack length $2c$. For one quarter of plate/pipe, the crack dimensions and other plate/pipe dimensions are input to the auto-mesh generation program. Then there generate 11 pieces of 8 wedge-shaped singular elements, and 8 elements in both radial and circumferential directions. The near crack-front FE mesh consists of approximately 3000 nodes and 700 C3D20 (ABAQUS Library, 1999) [5] elements. [Figs. 2(a)-(b)]. The FE mesh connecting this crack-front region with the rest part of plate/pipe, and the FE mesh for the rest part itself are further generated one after another. The entire 3-D FE models are shown in Figs. 2(c)-(d). The FE models consist of approximately 7500 nodes and 1500 C3D20 elements.

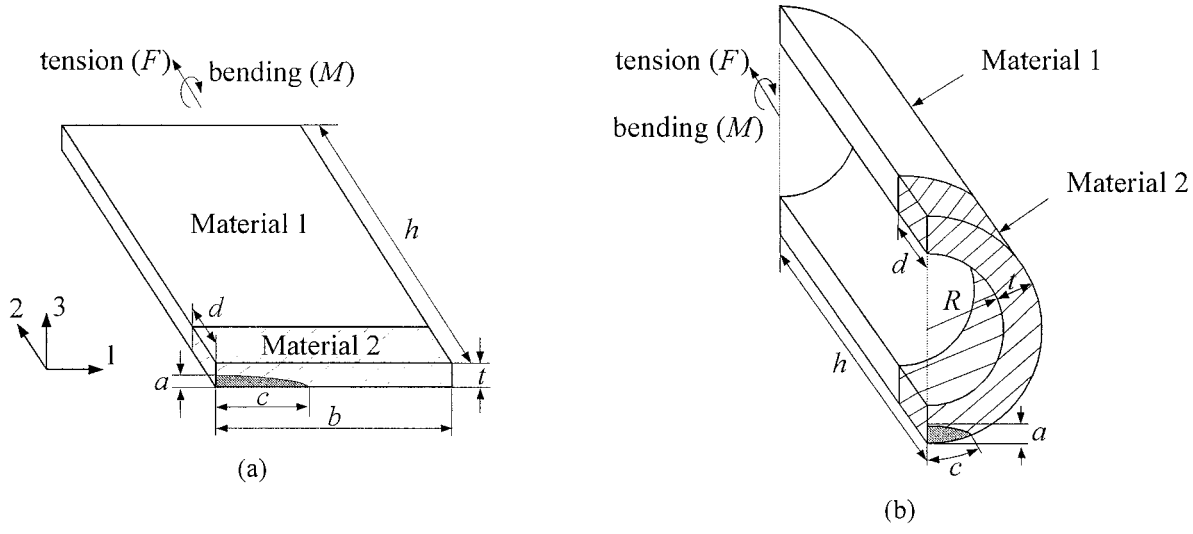

Fig. 1 Schematic diagram of one-quarter of a elliptical surface-cracked bimaterial (a) plate and (b) pipe.

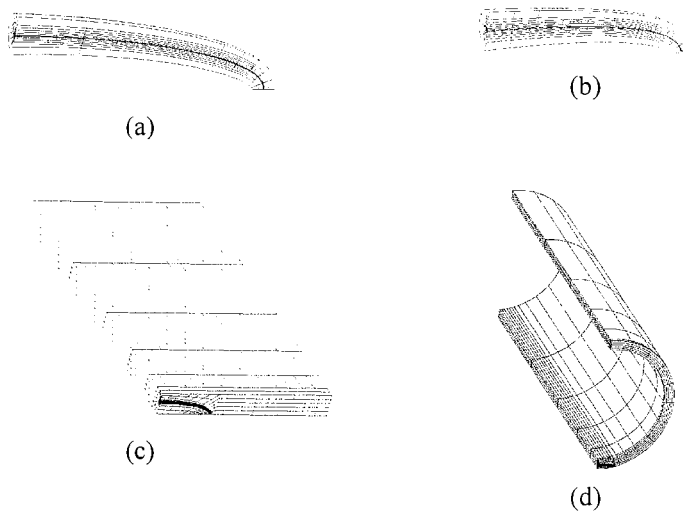

Fig. 2 The 3D mesh near the crack front of (a) plate (a/t = 0.6, a/c = 0.24), (b) pipe (a/t = 0.5, a/c = 0.3) and entire 3D mesh of elliptical surface-cracked (c) plate, (d) pipe.

Post-processing Program for *T*-stress Calculation

In order to calculate elastic T-stress of 2-D specimens under various loading conditions, several methods were suggested. The conceptually simplest one among them is to calculate T-stress in a straightforward manner from its definition.

$$\begin{bmatrix} \sigma_{xx} & \sigma_{xy} \\ \sigma_{yx} & \sigma_{yy} \end{bmatrix} = \frac{K_I}{\sqrt{2\pi r}} \begin{bmatrix} f_{xx}(\theta) & f_{xy}(\theta) \\ f_{yx}(\theta) & f_{yy}(\theta) \end{bmatrix} + \begin{bmatrix} T & 0 \\ 0 & 0 \end{bmatrix} \tag{1}$$

Suppose that the elastic stress field of 3-D surface crack-front can be expressed first two terms of Williams' eigen expansion (1). Then the elastic T-stress can be obtained as follows [6]:

$$T(\phi^i, r^i, \theta^i) = [\sigma_{xx}(\phi^i, r^i, \theta^i) - \sigma_{yy}(\phi^i, r^i, \theta^i)] - \frac{K_I(\phi^i)}{\sqrt{2\pi r^i}}[f_{xx}(r^i, \theta^i) - f_{yy}(r^i, \theta^i)] \tag{2}$$

Here i denotes node number in FE mesh, ϕ^i is angular position from Z-axis, and (r^i, θ^i) are cylindrical coordinates centered at the crack-tip in x-y plane. The x-y plane is the local plane normal to the crack-front [see Fig. 3(b)]. $\sigma_{xx}(\phi^i, r^i, \theta^i)$ is the stress component in x-direction. The corresponding stress intensity factor $K_I(\phi^i)$ is calculated from $J(\phi^i)$ obtained from the virtual crack extension/domain integral methods (ABAQUS) [5]. In Eq. (2), singular stress components are significantly larger than the nonsingular T-stress value which needs to be obtained. Hence slight inaccuracy of σ_{xx} may lead to a substantial error in calculated T-stress value. To resolve this problem, another normal singular stress σ_{yy} is adopted. The motivation is that the two singular terms σ_{xx} and σ_{yy} would offset the numerical inaccuracies and produce a number comparable to T.

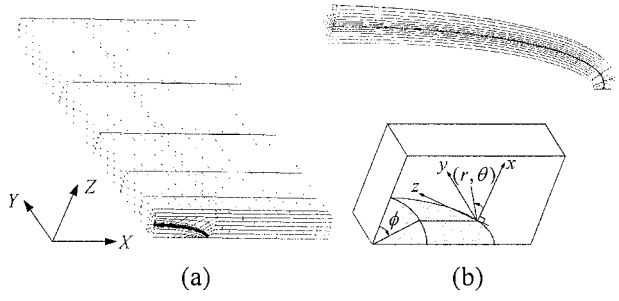

Fig. 3 3-D finite element model of the surface-cracked plate : (a) the entire 3D mesh and the global coordinate system (X-Y-Z) and (b) 3D mesh of crack-front field, and the local coordinate system (x-y-z).

On the above theoretical basis, we prepare a post-processing program to efficiently calculate T-stress along the crack-front from the stress fields obtained from 3-D elastic FE analyses. To validate our program, we compared our T-stress values with those from interaction integral by Nakamura and Parks [7]. Fig 4 shows the distribution of T-stress along the semi-elliptical surface crack-front in the plate under tensile and bending loads. Here $\sigma_a = F/bt$, far-field tensile stress and $\sigma_a = 6M/bt^2$, the maximum far-field bending stress [see Fig. 1(a)]. Under the tensile load, the difference between two solutions is less than 5% except near free surface region ($\phi = 90°$). Under bending, the difference between two solutions is less than 5% except near center region ($\phi = 0°$). We thus confirmed that T-values by two methods agree quite well with each other.

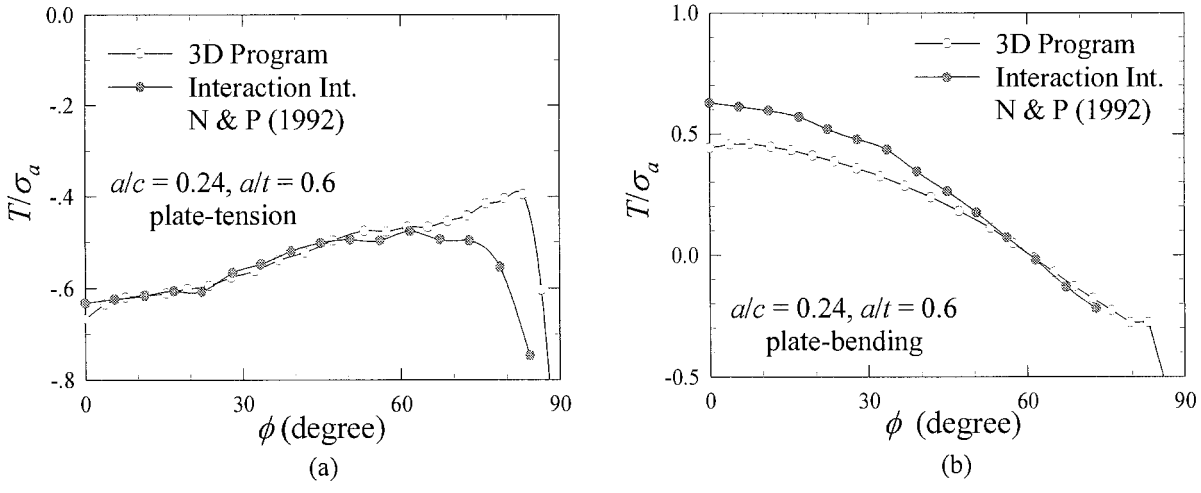

Fig. 4 Normalized T-distribution along the crack front of a deep-cracked plate evaluated by two different methods : (a) remote tension and (b) remote bending.

YIELD STRENGTH MISMATCHED WELDED JOINT

To satisfy the functional requirements, two different kinds of materials are often bonded together. Two different cases can be considered. One is the bimaterial with a bonded single interface. The other is the bimaterial with an intermediate material bonding the main materials at its both edges. This study focuses on the second case where a semi-elliptical surface crack resides on the symmetry plane of the intermediate material (Fig. 1). Unlike the crack-tip stress field of homogeneous material, that of bimaterial is strongly affected not only by specimen configuration and loading condition but also by mismatch of material properties.

Considering the symmetries of geometrical configuration and load, we model only one quarter of bimaterial plate and pipe with semi-elliptical surface cracks (Fig. 1). The 3D FE meshes were produced using the auto-mesh generation program described in the preceding chapter. The total height of plate is *2h*, the width *2b*, the total height of intermediate material *2d*, and the thickness *t*. The total length of pipe is *2h*, and the inner radius *R*, the total height of intermediate material *2d*, and the thickness *t*. The semi-elliptical surface crack is located on the center of the plate, and on the exterior of the pipe center. Also, the maximum crack depth is *a*, and the crack length 2*c*. The dimensions of plate are b/t = 8, h/t = 16, a/t = 0.6, a/c = 0.24, and t = 5mm. The dimensions of pipe are R/t = 6.67, h/t = 33.3, a/t = 0.5, a/c = 0.3, and t = 3mm.

Crack-tip Stress Field

Fig. 5 shows the variations of plane strain stress triaxiality ($\sigma_m/\sigma_0|_{\theta=0°}$) and crack opening stress ($\sigma_{22}/\sigma_0|_{\theta=0°}$) in an elastic-perfectly plastic material with *T*-stress change at the distance of $r = 2J/\sigma_0$ from the crack-tip [8]. The negative *T*-stress releases the crack-tip constraint significantly. Those FE stress solutions for elastic-perfectly plastic crack-tip fields can be recast as in the following forms.

$$-0.7 \le \tau \le 0.7\ ;\quad (\sigma_m/\sigma_0)_{\theta=0°} = C_1 + C_2\tau + C_3\tau^2 \tag{3a}$$

$$-0.7 \le \tau \le 0.7\ ;\quad (\sigma_{22}/\sigma_0)_{\theta=0°} = C_4 + C_5\tau + C_6\tau^2 \tag{3b}$$

Here $\tau = T/\sigma_0$, T is elastic *T*-stress, σ_0 is the yield strength, and (r, θ) are polar coordinates centered at the crack-tip. The regression coefficients are (C_1, C_2, C_3) = (2.26, 0.68, -0.81), (C_4, C_5, C_6) = (2.26+0.577, 0.68, -0.81).

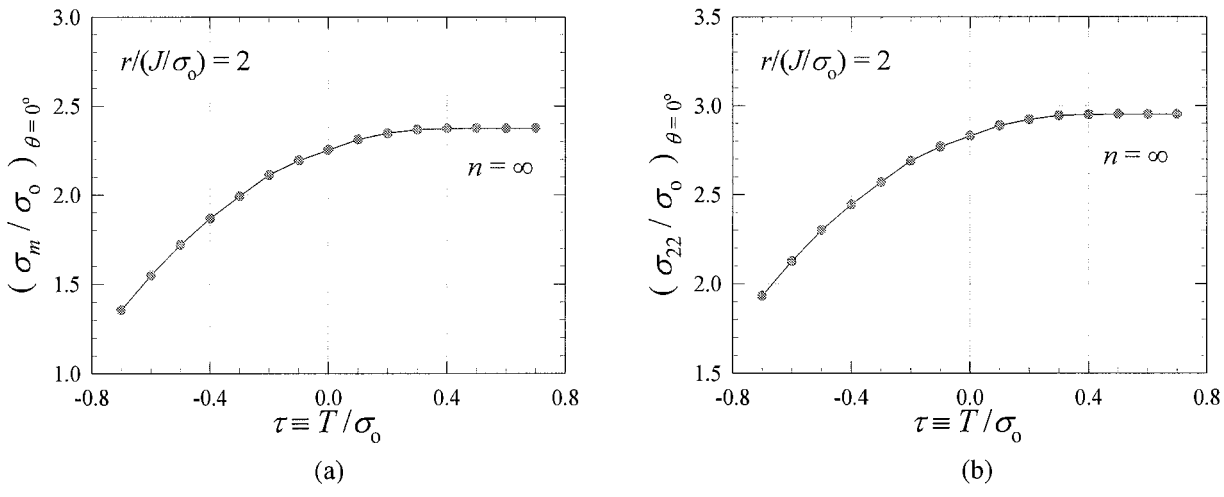

Fig. 5 Normalized (a) hydrostatic stress and (b) crack-tip opening stress at various values of *T*-stress for elastic-perfectly plastic material.

The Prandtl stress-field [9], deep within the crack-tip plastic zone in an elastic-perfectly plastic homogeneous material, consists of tri-regions (I, II, III) as shown in Fig. 6. The stress state of region I ($135° \le \theta \le 180°$) is derived to be homogeneous (uniform) from the yielding and free surface conditions. The range of θ is referred to the upper half with the symmetry considered, and k ($= \sigma_0/\sqrt{3}$) denotes the yield strength in shear.

$$\sigma_{rr} = k\,(1+\cos 2\theta) \tag{4a}$$
$$\sigma_{\theta\theta} = k\,(1-\cos 2\theta) \tag{4b}$$
$$\sigma_{zz} = \sigma_m = k \tag{4c}$$
$$\sigma_{r\theta} = k\,\sin 2\theta \tag{4d}$$

In the fan-region II ($45^\circ \le \theta \le 135^\circ$), σ_m changes with angular position according to the Hencky's equation of equilibrium ($d\sigma_m = -2\,k d\theta$), and the stress state of fan-region II is shown below.

$$\sigma_{rr} = \sigma_{\theta\theta} = \sigma_{zz} = \sigma_m = k(1+3\pi/2-2\theta) \tag{5a}$$
$$\sigma_{r\theta} = k \tag{5b}$$

The region III ($0^\circ \le \theta \le 45^\circ$) just ahead of the crack-tip shows the uniform stress state again as follows.

$$\sigma_{rr} = k\,(\pi+1-\cos 2\theta) \tag{6a}$$
$$\sigma_{\theta\theta} = k\,(\pi+1+\cos 2\theta) \tag{6b}$$
$$\sigma_{zz} = \sigma_m = k\,(\pi+1) \tag{6c}$$
$$\sigma_{r\theta} = k\,\sin 2\theta \tag{6d}$$

Of particular interesting point is, at the crack-tip ahead angular position $\theta = 0^\circ$ in region III, $\sigma_{\theta\theta} = \sigma_{22} = k(\pi+2)$ and $\sigma_m = k(\pi+1)$ from Eqs. (6). Therefore, the difference of two stress values is simply k. For this reason, the difference between triaxiality of Eq. (3a) and crack opening stress of Eq. (3b) is $k = 0.577\sigma_o$.

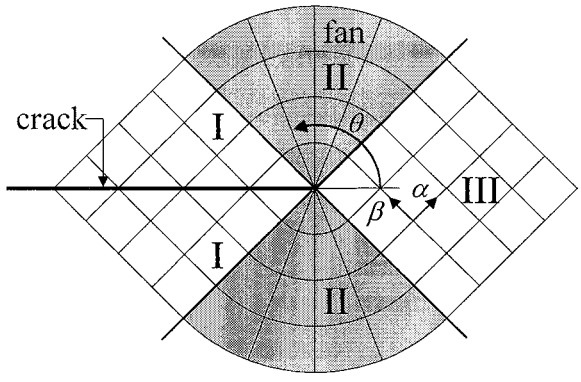

Fig. 6 The Prandtl slip line field.

Semi-elliptical Surface Cracked Plate

Considering the symmetries of geometrical configuration and load, we model only one quarter of plate with a semi-elliptical surface crack [Fig. 1(a)]. We examine the stress triaxiality and crack opening stress with respect to the magnitude of applied load via elastic-plastic FE analyses. Effect of yield strength on the stress field is focused in the investigation. We also validate the *J-T* approach by comparing the 3D elastic-plastic FE stress solutions with the *J-T* predictions. The dimensions of plate are b/t = 8, h/t = 16 and a/t = 0.6, a/c = 0.24, d/t = 1, and t = 5mm.

For an elastic-perfectly plastic homogeneous cracked plate with given configuration, the magnitude of applied tensile load is varied as 0.2, 0.26, 0.49, and 0.6 of the limit load of uncracked plate. For elastic-perfectly plastic bimaterials with yield strength ratios $[(\sigma_o|_2)/(\sigma_o|_1)]$ = 1.5 and 2, the magnitude of applied tensile load is set to 0.6 of the limit tensile load of uncracked plate. As the magnitude of applied load, (Σ^∞), refers to the uncracked plate, the net load on the ligament of cracked plane, (Σ_n^∞), is approximately 1.2 times the far-field apparent load ($\Sigma^\infty = 0.6 \leftrightarrow \Sigma_n^\infty = 0.72$). Figs. 7(a)-(b) show the ratios of the stress triaxiality and crack opening stress at $r = 2J/\sigma_o$ from FE analyses to those from the *J-T* predictions by Eqs. (3a)-(3b), for various magnitudes of applied tensile load. The *T*-stress used in *J-T* prediction is obtained by "elastic" FE analyses of given plate with the same magnitude of tensile load for elastic-plastic analysis. The *J-T* prediction

of triaxiality is more accurate at smaller load level. Errors in *J-T* prediction in homogeneous material [solid lines in Fig. 7(a)] at all examined load levels are less than 10% except near free surface ($\phi \simeq 90°$). Moreover, the triaxialities of bimaterials are higher than those of homogeneous material, resulting in smaller errors at load level of 0.6 [dashed and dotted lines in Fig. 7(a)] in this tensile loading case. The *J-T* prediction of crack opening stress is also more accurate at smaller load level. Errors in *J-T* prediction of σ_{22} in homogeneous material [solid lines in Fig. 7(b)] for all examined load levels are less than 3% except near free surface ($\phi \simeq 90°$). Crack opening stresses of bimaterials are higher than those of homogeneous material, also resulting in smaller errors [dashed and dotted lines in Fig. 7(b)] in this tensile loading case.

For an elastic-perfectly plastic homogeneous cracked plate with given configuration, the magnitude of applied bending load is varied as 0.38 and 0.6 of the limit load of uncracked plate. For elastic-perfectly plastic bimaterials with yield strength ratios $[(\sigma_o|_2)/(\sigma_o|_1)] = 1.5$ and 2, the magnitude of applied bending load is set to 0.6 of the limit bending load of uncracked plate. Figs. 7(c)-(d) show the ratios of the stress triaxiality and crack opening stress at $r = 2J/\sigma_o$ from FE analyses to those from the *J-T* predictions by Eqs. (3a)-(3b), for various magnitudes of applied bending load. The *T*-stress for *J-T* prediction is also obtained by "elastic" FE analyses of given plate with the same magnitude of bending load for elastic-plastic analysis. Errors in *J-T* prediction are less than 10% except near crack center ($\phi \simeq 0°$) in both homogeneous material [solid lines in Fig. 7(c)] at two examined load levels and bimaterials at load level of 0.6 [dashed and dotted lines in Fig. 7(c)]. Errors in *J-T* prediction of σ_{22} are less than 7% except near crack center ($\phi \simeq 0°$) in both homogeneous material [solid lines in Fig. 7(d)] at two examined load levels and bimaterials at load level of 0.6 [dashed and dotted lines in Fig. 7(d)]. The *J*-value at the crack center under plate-bending load is relatively smaller than the neighbor region in a deeply cracked (a/t = 0.6) configuration. We thus presume that the location of $r = 2J/\sigma_o$ becomes rather close to the crack-tip, which may leads to a sizable numerical inaccuracy. That is, if relatively small bending load acts on the plate with high yield strength and a deep crack, *J-T* prediction error may become larger. The *J-T* prediction of σ_{22} is overall a bit more accurate than that of σ_m in both homogeneous materials and bimaterials as observed in Fig. 7.

Semi-elliptical Surface Cracked Pipe

Considering the symmetries of geometrical configuration and load, we model only one quarter of pipe with a semi-elliptical surface crack [Fig. 1(b)]. The dimensions of pipe are R/t = 6.67, h/t = 33.3 and a/t = 0.5, a/c = 0.3, d/t = 1, and t = 3mm. For an elastic-perfectly plastic homogeneous cracked pipe with given configuration, the magnitude of applied tensile load is varied as 0.21, 0.39, and 0.6 of the limit load of uncracked pipe. For elastic-perfectly plastic bimaterials with yield strength ratios $[(\sigma_o|_2)/(\sigma_o|_1)] = 1.5$ and 2, the magnitude of applied tensile load is set to 0.6 of the limit tensile load of uncracked pipe. Figs. 8(a)-(b) show the ratios of the stress triaxiality and crack opening stress at $r = 2J/\sigma_o$ from FE analyses to those from the *J-T* predictions by Eqs. (3a)-(3b), for various magnitudes of applied tensile load. The *T*-stress used in *J-T* prediction is obtained by "elastic" FE analyses of the given pipe with the same magnitude of tensile load for elastic-plastic analysis. In case of pipe-tension, the features of *J-T* prediction are very similar to those of plate-tension, as expected by intuition.

In case of pipe-bending, however, larger structural bending stiffness of pipe leads to quite different aspects in *J-T* prediction from those in plate-bending. For an elastic-perfectly plastic homogeneous cracked pipe with given configuration, the magnitude of applied bending load is varied as 0.28, 0.51, and 0.6 of the limit load of uncracked pipe. For elastic-perfectly plastic bimaterials with yield strength ratios $[(\sigma_o|_2)/(\sigma_o|_1)] = 1.5$ and 2, the magnitude of applied bending load is set to 0.6 of the limit bending load of uncracked pipe. Figs. 8(c)-(d) show the ratios of σ_m and σ_{22} at $r = 2J/\sigma_o$ from FE analyses to those from the *J-T* predictions by Eq. (3), for various magnitudes of applied bending load. Unlike the plate-bending, the *J-T* prediction is more accurate around the crack center ($\phi \simeq 0°$). In short, the features of *J-T* prediction in pipe-bending are much more like those in plate/pipe-tension. Errors in *J-T* prediction of σ_m are less than 10% except near free surface ($\phi \simeq 90°$) in both homogeneous material [solid lines in Fig. 8(c)] at two examined load levels and bimaterials at load level of 0.6 [dashed and dotted lines in Fig. 8(c)]. Errors in *J-T* prediction of σ_{22} are less than 7% except near free surface ($\phi \simeq 90°$) in both homogeneous material [solid lines in Fig. 8(d)] at two examined load levels and bimaterials at load level of 0.6 [dashed and dotted lines in Fig. 8(d)].

We thus far have compared the actual 3-D elastic-plastic stress fields along the crack-front to those by *J-T* prediction for surface-cracked plates and pipes under tensile and bending loads, thereby demonstrating the extended validity of *J-T* approach. It is noteworthy that around free surface region ($\phi = 90°$), both near plane stress condition and complex geometrical configuration restrain the *J-T* approach from accurately predicting crack-tip stress fields, because Eq. (3a)-(3b) are based on plane strain FE solutions.

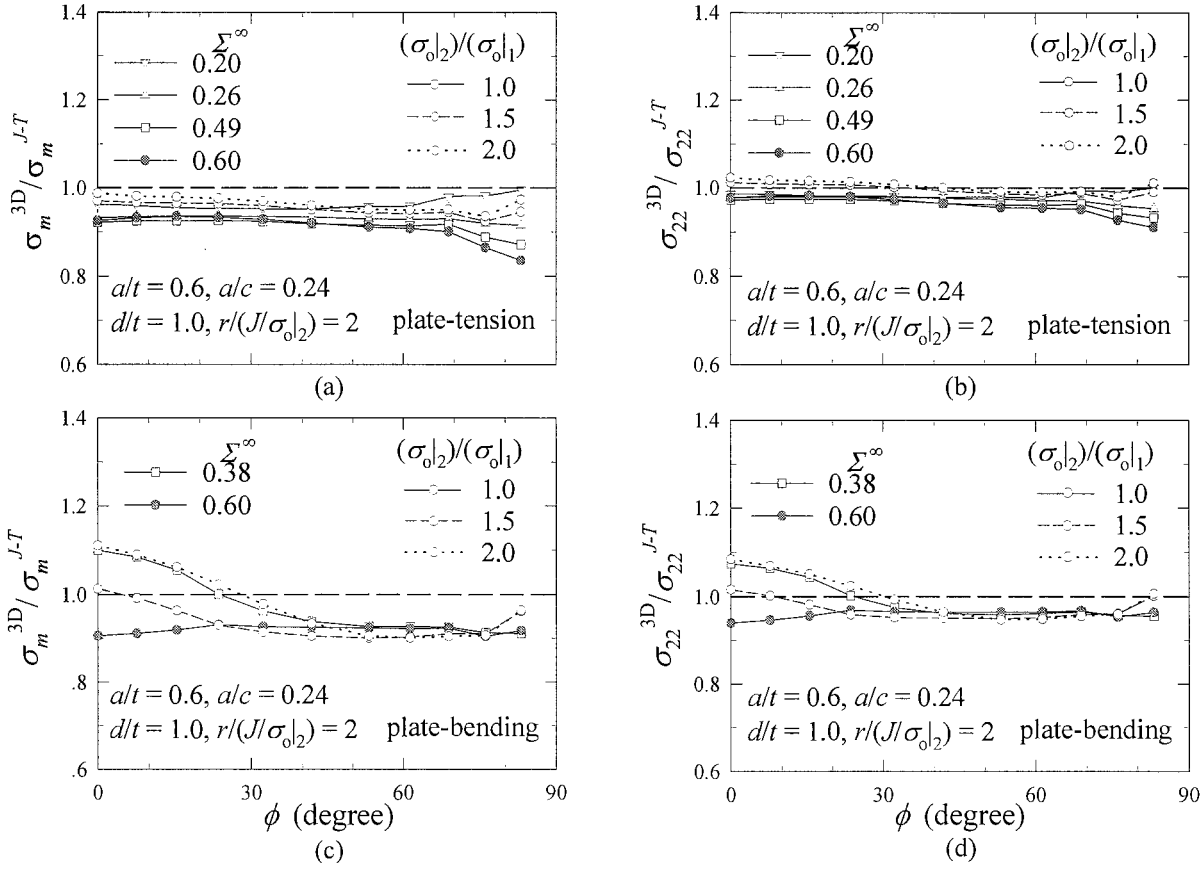

Fig. 7 Hydrostatic and crack-tip opening stress normalized by the *J-T* solution of plate under remote tension [(a), (b)], and bending [(c), (d)] for various load levels & materials.

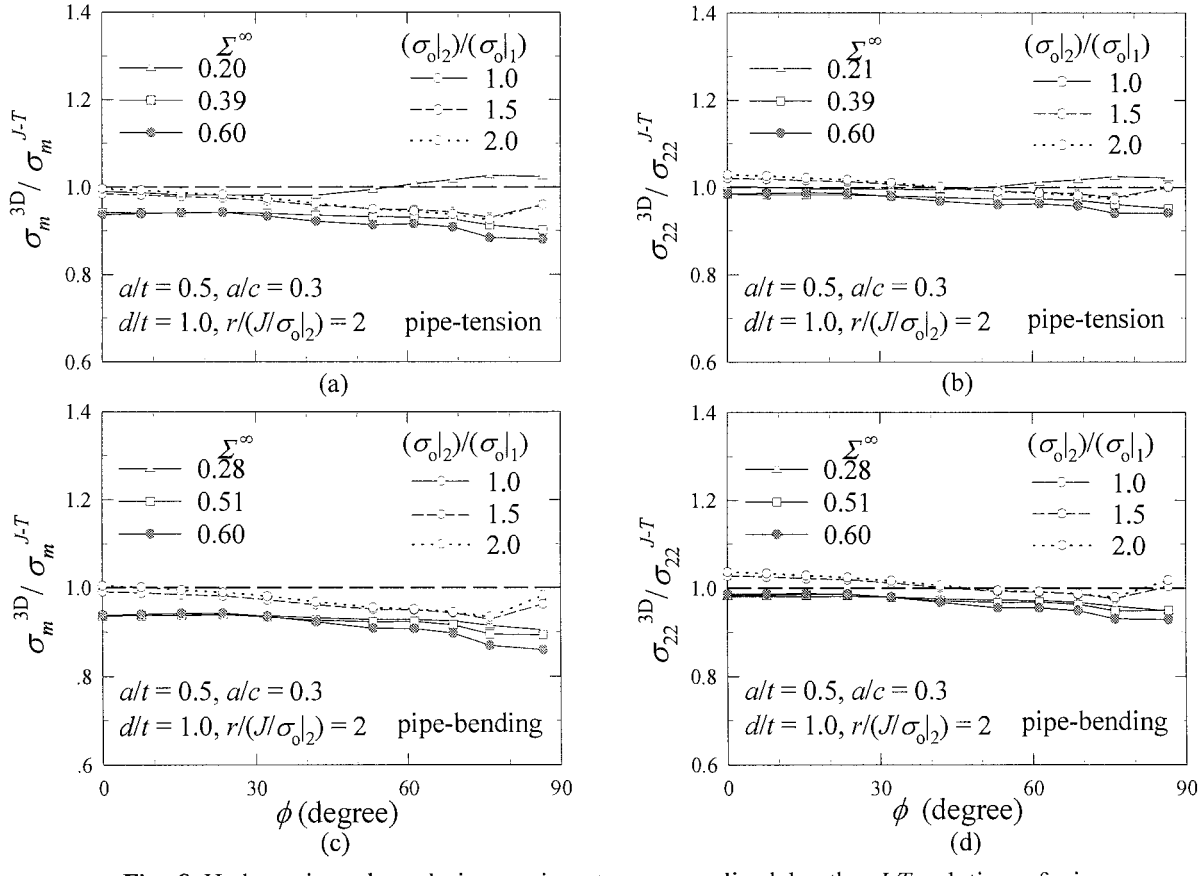

Fig. 8 Hydrostatic and crack-tip opening stress normalized by the *J-T* solution of pipe under remote tension [(a), (b)], and bending [(c), (d)] for various load levels & materials.

CONCLUDING REMARKS

We developed an automatic 3-D FE mesh generation program for plates and pipes with semi-elliptical surface cracks, and a post-processing program to calculate *T*-stress along the crack-front. With those pre/post-programs, we effectively studied the effect of plastic strength mismatch on the stress field of semi-elliptical surface cracks in the bimaterial plates and pipes, in terms of *J-T*. From those studies, the following concluding remarks are made.

(1) For analyzed semi-elliptical surface cracks in plate-tension, pipe-tension and pipe-bending, the cracks undergo so low constraint that use of only single parameter brings about conservative results.

(2) The *J-T* approach using Eqs. (3a)-(3b) provides quite accurate elastic-plastic stress fields along most of the surface crack-front within an error of about 10%.

ACKNOWLEDGMENTS

The author is grateful for the support provided by a grant from the Korea Science & Engineering Foundation, and Safety and Structural Integrity Research Center

REFERENCES

1. Larsson, S. G. and Carlsson, A. J., 1973, "Influence of Non-singular Stress Terms and Specimen Geometry on Small-scale Yielding at Crack Tips in Elastic-plastic Material," *Journal of the Mechanics and Physics of Solids*, Vol. 21, pp. 263-277.
2. Williams, M. L., 1957, "On the Stress Distribution at the Base of a Stationary Crack," *Journal of Applied Mechanics*, Vol. 24, pp. 111-114.
3. Rice, J. R., 1974, "Limitations to the Small-scale Yielding Approximation for Crack-tip Plasticity," *Journal of the Mechanics and Physics of Solids*, Vol. 22, pp. 17-26.
4. Betegon, C. and Hancock, J. W., 1991, "Two-parameter Characterization of Elastic-plastic Crack Tip Fields," *Journal of Applied Mechanics*, Vol. 58, pp. 104-110.
5. ABAQUS *User's Manual*, 1999, Version 5.8 Hibbitt, Karlsson and Sorensen, Inc., Pawtucket, RI.
6. Wang, Y. Y., 1991, *A Two-parameter Characterization of Elastic-plastic Crack Tip Fields and Applications to Cleavage Fracture*, Chapters 1-4, Ph. D. Dissertation, Department of Mechanical Engineering, Massachusetts Institute of Technology.
7. Nakamura, T. and Parks, D. M., 1992, "Three- Dimensional Stress Field Near the Crack Front of a Thin Elastic Plate," *Journal of Applied Mechanics*, Vol. 55, pp. 805-813.
8. Lee, H. and Kim, Y-J, 2001, "Interfacial Crack-Tip Constraints and *J*-integrals in Plastically Mismatched Bimaterials," *Engineering Fracture Mechanics*, In Print.
9. Du, Z. Z. and Hancock, J. W., 1991, "The Effect of Non-singular Stresses on Crack-tip Constraint," *Journal of the Mechanics and Physics of Solids*, Vol. 39, No. 4, pp. 555-567.